Static dielectric response of the electron gas

C. Bowen*
Lawrence Livermore National Laboratory, Livermore, California 94550
and Department of Applied Science, University of California, Davis, California 95616

G. Sugiyama
Lawrence Livermore National Laboratory, Livermore, California 94550

B.J. Alder
Lawrence Livermore National Laboratory, Livermore, California 94550
and Department of Applied Science, University of California, Davis, California 95616
(Received 7 April 1994; revised manuscript received 25 July 1994)

We determine the static dielectric function of the electron gas at selected densities by using variational and fixed-node diffusion quantum Monte Carlo to find the response to a sinusoidal electric field. The dielectric function is then calculated by relating the induced charge density to the change in ground-state energy as a function of the amplitude of the applied field. A released-node Green's-function Monte Carlo calculation shows that the diffusion results are exact within the determined error bars, apart from the size dependence correction for extrapolation to the thermodynamic limit. The dielectric response is consistent at long wavelengths with the compressibility sum rule derived from a fit to Ceperley and Alder's Green's-function Monte Carlo results, but exhibits differences from accepted dielectric models at intermediate wave vectors.

I. INTRODUCTION

In this paper, we determine the static dielectric function of the electron gas $\epsilon(\mathbf{q})$ at selected wave vectors $\mathbf{q}$ for several paramagnetic fluid densities. The electron gas is uniquely characterized by the dimensionless density parameter $r_s = r_0/a_0$, which is a measure of the relative strengths of the Coulomb and kinetic energies (r_0 is the Wigner-Seitz radius, related to the electronic density n by $4\pi r_0^3/3 = 1/n$ and a_0 is the Bohr radius). An understanding of the electrostatic response of the electron gas as a function of r_s yields insight into the screening properties of metals and alloys, including Friedel oscillations and the renormalization of phonon frequencies.

The dielectric function is defined in terms of the electronic response to an external perturbation. This is readily calculable only in the weak-coupling regime ($r_s \ll 1$), where the electrons may be treated as uncorrelated. The response can then be found by solving for the one-electron density matrix in the Hartree self-consistent field of the external perturbation and the induced electronic charge — the random-phase approximation (RPA). For densities of physical interest, ranging from the metallic state ($2 \lesssim r_s \lesssim 6$) to the Wigner crystallization regime ($r_s \gtrsim 100$), the RPA fails, since it does not properly account for the exchange and correlation hole around each electron. Following Hubbard's introduction of a correction factor to the RPA, improved expressions for the dielectric at these densities have been found using field-theoretic techniques,[1] solutions of the equations of motion for the Wigner distribution function,[2] self-consistent schemes,[3–5] semiempirical fits,[6] and numerical solutions of the Fermi hypernetted-chain equations.[7,8] However, the effect and range of applicability of the approximations involved in these approaches are difficult to establish *a priori*, making a first-principles calculation desirable.

The quantum Monte Carlo method has successfully obtained ground-state properties of charged quantum fluids and solids[9,10] by taking correlation contributions into account exactly. The viability of using the method to obtain the static dielectric response was demonstrated by the present authors in a calculation for the charged Bose fluid spanning the entire range of densities, from the Bose-condensed phase to the Wigner crystallization regime.[11] A similar approach has also been used to determine the response functions of ^{4}He and the electron gas in two dimensions.[12]

In Sec. II, we describe several dielectric models and introduce the energy difference method of calculating the dielectric response. This is followed by a review of quantum Monte Carlo (QMC) methods in Sec. III. Our results are then presented and summarized in Secs. IV and V.

II. DIELECTRIC FUNCTION

The static dielectric function is a measure of the linear response induced in a system by a charge perturbation; the perturbation is assumed small enough so that higher-order terms in the response do not occur. In terms of the external, induced, and total charge densities ρ, or, equivalently, in terms of the electric field $\mathbf{E}$ and displacement $\mathbf{D}$ or the corresponding potentials ϕ,

$$\frac{1}{\epsilon(\mathbf{q})} \equiv \frac{\mathbf{E}(\mathbf{q})}{\mathbf{D}(\mathbf{q})} = \frac{\phi_{\text{total}}(\mathbf{q})}{\phi_{\text{ext}}(\mathbf{q})} = \frac{\rho_{\text{total}}(\mathbf{q})}{\rho_{\text{ext}}(\mathbf{q})} = 1 + \frac{\rho_{\text{ind}}(\mathbf{q})}{\rho_{\text{ext}}(\mathbf{q})} . \quad (2.1)$$

The fields, potentials, and charge densities in this equation are quantum statistical averages satisfying the microscopic Maxwell equations in Fourier space:

$$\begin{aligned} i\mathbf{q}\cdot\mathbf{D}(\mathbf{q}) &= -q^2\phi_{\text{ext}}(\mathbf{q}) = 4\pi\rho_{\text{ext}}(\mathbf{q}), \\ i\mathbf{q}\cdot\mathbf{E}(\mathbf{q}) &= -q^2\phi_{\text{total}}(\mathbf{q}) = 4\pi\rho_{\text{total}}(\mathbf{q}) \\ &= 4\pi[\rho_{\text{ext}}(\mathbf{q}) + \rho_{\text{ind}}(\mathbf{q})]. \end{aligned} \quad (2.2)$$

The self-consistent field (SCF) or RPA dielectric function applicable at high densities is

$$\epsilon_{\text{SCF}}(\mathbf{q}) = 1 - \frac{4\pi e^2}{\Omega q^2} \sum_{\mathbf{k}} \frac{f_0(E_{\mathbf{k}+\mathbf{q}}) - f_0(E_{\mathbf{k}})}{E_{\mathbf{k}+\mathbf{q}} - E_{\mathbf{k}}} , \quad (2.3)$$

where the sum is over the plane wave basis set, e is the electronic charge, Ω is the volume occupied by the electron gas, $E_{\mathbf{k}}$ is the kinetic energy, and $f_0(E_{\mathbf{k}})$ is the free-electron Fermi distribution function. In the ground state, this sum may be replaced by an integration up to the Fermi level, $k_F = (3\pi^2 n)^{1/3}$, yielding the Lindhard dielectric function

$$\epsilon_{\text{LIND}}(\mathbf{q}) = 1 - \chi_{\text{LIND}} = 1 + \frac{k_s^2}{2q^2}\left[1 + \frac{1}{2x}(1-x^2)\ln\left|\frac{1+x}{1-x}\right|\right], \quad (2.4)$$

where $1/k_s$ is the Thomas-Fermi screening length, $k_s^2 = 4(3n/\pi)^{1/3}/a_0$, and $x = q/2k_F$.

Improvements on the Lindhard dielectric are typically expressed in terms of the local-field correction $G(q)$, defined by

$$\epsilon(\mathbf{q}) = 1 - \frac{\chi_{\text{LIND}}}{1 + G(q)\,\chi_{\text{LIND}}}, \quad (2.5)$$

which attempts to take into account the exchange and correlation hole. The short-wavelength behavior of $G(q)$ is given by the Kimball relation,[13]

$$\lim_{q\to\infty} G(q) = 1 - g(0) , \quad (2.6)$$

where $g(0)$ is the pair correlation function at zero separation. At long wavelengths, the dielectric function is related to the thermodynamic compressibility κ by the compressibility sum rule[14]

$$\lim_{q\to 0} \epsilon(\mathbf{q}) = 1 + \left(\frac{k_s}{q}\right)^2 \frac{\kappa}{\kappa_{\text{free}}} , \quad (2.7)$$

where κ_{free} is the compressibility of the noninteracting electron gas. The compressibility ratio is in turn related to the correlation energy per electron $E_c(r_s)$ by

$$\frac{\kappa}{\kappa_{\text{free}}} = \left(1 - \frac{4\alpha}{\pi} r_s\gamma_0\right)^{-1} , \quad (2.8)$$

$$\gamma_0 = \frac{1}{4} - \frac{\pi\alpha}{24} r_s^5 \frac{d}{dr_s}\left[r_s^{-2}\frac{d}{dr_s}E_c(r_s)\right] , \quad (2.9)$$

where $\alpha \equiv (4/9\pi)^{1/3}$ and the energies are in Ry.

Vashishta and Singwi[3] used a self-consistent solution relating $G(q)$, the static structure factor, and the frequency-dependent dielectric function to obtain a formula applicable in the metallic density regime

$$G(q) = a\left[1 - e^{-b(q/k_F)^2}\right], \quad (2.10)$$

where a and b are density-dependent fitting parameters. Ichimaru and Utsumi[6] fit an elaborate functional form for $G(q)$,

$$G(q) = aQ^4 + bQ^2 + c + \left[aQ^4 + \left(b + \frac{8}{3}\right)Q^2 - c\right] \times \left(\frac{4-Q^2}{4Q}\right)\ln\left|\frac{2+Q}{2-Q}\right| , \quad (2.11)$$

$$a = 0.029 \quad (0 \le r_s \le 15) , \quad (2.12)$$

$$b = \frac{9}{16}\gamma_0 - \frac{3}{64}[1 - g(0)] - \frac{16}{15}a , \quad (2.13)$$

$$c = -\frac{3}{4}\gamma_0 + \frac{9}{16}[1 - g(0)] - \frac{16}{5}a , \quad (2.14)$$

where $Q = q/k_F$. γ_0 was obtained from the Padé fit of Vosko, Wilk, and Nusair[15] to Ceperley and Alder's released-node Green's-function Monte Carlo (GFMC) energies for the electron gas[9] while $g(0)$ was taken from Yasuhara's expression[16]

$$g(0) = \frac{1}{8}\left[\frac{z}{I_1(z)}\right]^2 , \quad z \equiv 4(\alpha r_s/\pi)^{1/2} , \quad (2.15)$$

in terms of the first-order modified Bessel function $I_1(z)$. The parameter a was chosen to closely reproduce the authors' microscopic theory.[4]

Based on the hypernetted-chain method, Pietiläinen and Kallio[8] proposed a relationship between the structure factor $S(k)$ and the local-field correction

$$S(k) = \frac{1}{\{1 + 12r_s[1 - G(k)]/(r_o k)^4\}^{1/2}}, \quad (2.16)$$

which yields the uniform limit results as $k \to 0$. The degree of validity of this self-consistent condition depends on the accuracy of the Lado approximation for the squared Slater determinant.

The dielectric function can be determined from the response of the electron gas to an external field of strength A, produced by a sinusoidal deformation of the neutralizing positive background. The Hamiltonian of this problem is

$$\begin{aligned} H &= H_0 + H_{\text{ext}}, \\ H_0 &= -\frac{1}{r_s^2}\sum_{i=1}^{N}\nabla_i^2 + \frac{2}{r_s}\sum_{i<j}^{N}\frac{1}{r_{ij}} , \\ H_{\text{ext}} &= A\sum_{i=1}^{N}\cos(\mathbf{q}\cdot\mathbf{r}_i) = e\sum_{i=1}^{N}\phi_{\text{ext}}(\mathbf{r}_i) , \end{aligned} \quad (2.17)$$

where N is the number of electrons and $r_{ij} = |\mathbf{r}_i - \mathbf{r}_j|$. (Henceforth, lengths and energies will be quoted in units

of r_0 and Ry, respectively, with $k_F = 1/\alpha \approx 1.92$.) The charge density induced by the field is given by the difference in the expectation values of the density operator in the presence and absence of the perturbation,

$$\rho_{\rm ind}(\mathbf{q}) = \langle \rho_{\mathbf{q}} \rangle_A - \langle \rho_{\mathbf{q}} \rangle_0 = \frac{e}{\Omega} \left[\left\langle \sum_{i=1}^{N} e^{-i\mathbf{q}\cdot\mathbf{r}_i} \right\rangle_A - \left\langle \sum_{i=1}^{N} e^{-i\mathbf{q}\cdot\mathbf{r}_i} \right\rangle_0 \right] . \quad (2.18)$$

It can be related to the second derivative of the ground-state energy E_0 with respect to the amplitude of the applied field (cf. Ref. 11), leading to the following expression for the dielectric function:

$$\frac{1}{\epsilon(\mathbf{q})} = 1 + \frac{12}{N r_s} \frac{1}{q^2} \frac{d^2 E_0(A)}{dA^2} . \quad (2.19)$$

This formula is used in our calculations since it is particularly well suited to quantum Monte Carlo, which accurately calculates ground-state energies from first principles. As discussed in our study of the boson dielectric response, determination of the induced charge by direct measurement of $\rho_{\rm ind}(\mathbf{q})$ requires much longer QMC runs to obtain accurate convergence. Use of the Kubo relation for the imaginary-time density-density correlation function requires the extraction of dynamics, which poses a difficult problem in ground-state simulations.

The second derivative of the energy can be found from a quadratic fit, with the term linear in A omitted by symmetry arguments. Field strengths should be as small as possible, consistent with statistically meaningful energy differences, in order to insure linearity of the response. Linearity can then be tested for each applied field by checking that higher harmonics in the induced fluctuations do not appear. As a practical estimate of the linear regime, the field amplitudes used in our QMC simulations at $r_s = 4$ range from $\sim 0.5 - 2.0 \times 10^8$ V/cm, which is on the order of e/r_0^2.

III. QUANTUM MONTE CARLO

The ground-state energy is the minimum of the expectation value of the Hamiltonian H with respect to all possible trial wave functions $\Psi_T(\mathbf{R})$:

$$E_0 = \min_{\Psi_T(\mathbf{R})} \frac{\int \Psi_T^*(\mathbf{R}) H \Psi_T(\mathbf{R}) d\mathbf{R}}{\int |\Psi_T(\mathbf{R})|^2 d\mathbf{R}} , \quad (3.1)$$

where the integration is over the $3N$ particle coordinates $\mathbf{R} = (\mathbf{r}_1, \mathbf{r}_2, \ldots, \mathbf{r}_N)$. Variational Monte Carlo[17] uses the Metropolis algorithm to evaluate the integrals by sampling configurations $\mathbf{R}_j$ drawn from the probability density $P(\mathbf{R}) = \frac{|\Psi_T(\mathbf{R})|^2 d\mathbf{R}}{\int |\Psi_T(\mathbf{R})|^2 d\mathbf{R}}$. The variational energy $E_{\rm var}$ is then given by

$$E_0 \le E_{\rm var} = \lim_{M\to\infty} \frac{1}{M} \sum_{j=1}^{M} E_L(\mathbf{R}_j) ,$$

where $E_L(\mathbf{R}) = H\Psi_T(\mathbf{R})/\Psi_T(\mathbf{R})$ is the local energy. The variation is typically performed on a subset of wave functions to optimize a set of free parameters with the resulting $E_{\rm var}$ being a strict upper bound for E_0 within statistical error bars.

The diffusion Monte Carlo (DMC) algorithm[18] solves the imaginary-time many-body Schrödinger equation in the short time-step approximation. For computational efficiency, the equation is rewritten in terms of the mixed distribution $f(\mathbf{R},\tau) = \Psi(\mathbf{R},\tau)\Psi_T(\mathbf{R})$ as

$$\frac{\partial f}{\partial \tau} = \sum_{i=1}^{N} \left[\frac{\hbar^2}{2m} \nabla_i^2 f - \nabla_i \cdot (f \nabla_i \ln |\Psi_T|^2) \right] - \left(\frac{H\Psi_T}{\Psi_T} - E_T \right) f , \quad (3.2)$$

where E_T is an introduced constant known as the trial energy. The DMC solution is obtained by using the short time-step propagator

$$G(\mathbf{R} \to \mathbf{R}', \tau) = \left[\frac{4\pi\tau\hbar^2}{2m} \right]^{-3N/2} \times \exp \left[- \frac{\left[\mathbf{R}' - \mathbf{R} - \frac{\tau\hbar^2}{2m} \nabla \ln |\Psi_T(\mathbf{R})|^2 \right]^2}{\frac{4\tau\hbar^2}{2m}} \right] \times \exp \left[-\tau \left[E_L(\mathbf{R}) + E_L(\mathbf{R}') \right] /2 + \tau E_T \right]$$

to evolve an initial ensemble of configurations generated from a variational simulation according to

$$f(\mathbf{R}', t+\tau) = \int d\mathbf{R}\, G(\mathbf{R} \to \mathbf{R}', \tau) f(\mathbf{R}', t),$$

$$f(\mathbf{R}, 0) = |\Psi_T|^2 . \quad (3.3)$$

In the absence of symmetry constraints on the wave function, such as those imposed by fermion statistics, the asymptotic solution converges exponentially fast to the ground state. Extrapolation to $\tau \to 0$ then eliminates the short time-step approximation.

The mixed distribution f is interpreted as the density of diffusing configurations undergoing drift and branching processes. For fermion systems, antisymmetry is maintained by assuming that the ground-state wave function has the same (approximate) nodal structure as the trial function, so that the distribution never changes sign — the fixed-node approximation. The Schrödinger equation is then solved within the hypervolumes bounded by the nodal surface, by terminating any configuration that crosses it. The resulting DMC fixed-node energy can be shown to be a strict upper bound to the ground-state energy, and a very good one if the trial wave function is properly chosen.

The Green's-function Monte Carlo method[9,19] removes the time-step error of DMC by using the exact propagator instead of its short time-step approximation to evolve the probability distribution. The exact density matrix is generated from an expansion in terms of a trial density matrix, by iterative solution of a linear integral equa-

tion relating the two. In practice, a time-independent form of the propagator is used to evolve the configurations, the distribution after n propagation steps being known as the nth generation. Importance sampling and the fermion fixed-node approximation are introduced via the trial function described for DMC.

In the released-node method, the GFMC fixed-node distribution is considered to be an approximate starting population. Configurations are allowed to cross the nodes of the trial function and to continue for a few generations, but their contribution to any average changes sign at every node crossing. Antisymmetry is taken into account correctly, but the process is numerically unstable, since the distributions of configurations with either an even or odd number of node crossings both tend to the same unconstrained boson ground state, causing the evaluation of expectation values to become increasingly noisy. The node-crossing populations can be shown to grow exponentially with generation number, due to the difference between the Fermi and Bose energies of the system. Therefore, the released-node method is restricted to systems for which the trial nodes can be accurately approximated, so that relaxation occurs quickly enough and the ground-state energy can be accurately projected.

In QMC, the choice of trial wave function is of critical importance for efficient convergence and fermion antisymmetrization. A standard Slater-Jastrow product form is used for the ground-state trial function

$$\Psi_T(\mathbf{R}) = |D(\mathbf{R},\mathbf{k})|^{\uparrow}|D(\mathbf{R},\mathbf{k})|^{\downarrow}\, J(r_{ij})\ , \tag{3.4}$$

where $|D(\mathbf{R},\mathbf{k})|^{\uparrow}$ and $|D(\mathbf{R},\mathbf{k})|^{\downarrow}$ are Slater determinants of plane waves $|\mathbf{k}\rangle = e^{i\mathbf{k}\cdot\mathbf{r}}$ for the spin up and down populations and $J(r_{ij})$ is the Jastrow factor derived within the RPA, which takes into account both the cusp condition as two electrons approach each other and the long-range correlations. This unparametrized form has been used successfully in determining properties of the electron gas and low-Z metals.[10,17] The allowed values of $\mathbf{k}$ are those reciprocal to the finite simulation cell, with the ground state of the system obtained by filling the N states of lowest energy. In order to reduce surface effects, the possible choices for N are restricted to those which correspond to filled or closed shells (a shell consists of all $\mathbf{k}$ values related by cubic symmetries). The closed shell values for double spin occupancy used in this study may be determined by inspection and are $N/2 = 7, 19, 27, 33, 57, 81$.

In the presence of the external field, an appropriate modification of the form of the ground-state trial function is required:

$$\Psi_T^A(\mathbf{R}) = |D(\mathbf{R},\mathbf{k}^A)|^{\uparrow}|D(\mathbf{R},\mathbf{k}^A)|^{\downarrow}\, J(r_{ij}) \times \exp\left(\gamma \sum_{i=1}^{N} \cos(\mathbf{q}\cdot\mathbf{r}_i)\right)\ . \tag{3.5}$$

A similar product form was used with good results in the hypernetted-chain study of Ref. 7. The components of this trial function are suggested by a trivial rewriting of the Hamiltonian,

$$H = \left[-\frac{1}{r_s^2}\sum_{i=1}^{N}\nabla_i^2 + H_{\text{ext}}/\epsilon_{\text{SCF}}\right] + \left[\frac{2}{r_s}\sum_{i<j}^{N}\frac{1}{r_{ij}} + H_{\text{ext}}\,(1-1/\epsilon_{\text{SCF}})\right]\ . \tag{3.6}$$

The second bracketed term contains the interaction energy and a reduced perturbation which can be matched with the two-body Jastrow and the one-body pseudopotential of the trial function, respectively. The first bracketed term is the Hamiltonian of noninteracting electrons in an external field shielded by ϵ_{SCF} [Eq. (2.3)]. An exact solution for the Slater determinant orbitals $|\mathbf{k}^A\rangle$ satisfying this Hamiltonian involves Mathieu functions, but to linear order in A,

$$|\mathbf{k}^A\rangle = |\mathbf{k}\rangle - \frac{Ar_s^2}{2\epsilon_{\text{SCF}}}\left[\frac{|\mathbf{k}+\mathbf{q}\rangle}{(\mathbf{q}+2\mathbf{k})\cdot\mathbf{q}} + \frac{|\mathbf{k}-\mathbf{q}\rangle}{(\mathbf{q}-2\mathbf{k})\cdot\mathbf{q}}\right]\ , \tag{3.7}$$

as derived from first-order perturbation theory. The one-body pseudopotential parametrized by γ is everywhere positive and does not change the nodal surface of the system determined by the SCF orbitals. This suggests that γ may be found from the boson RPA solution[11] for an external field of strength $H_{\text{ext}}\,(1-1/\epsilon_{\text{SCF}})$:

$$\gamma = \frac{-Ar_s^2}{(q^4+12r_s)^{1/2}}\,(1-1/\epsilon_{\text{SCF}})\ . \tag{3.8}$$

This value of γ lies close to the optimal value as determined by variational minimization. An alternative trial function form, Eq. (3.7) with ϵ_{SCF} replaced by a variational parameter and $\gamma = 0$, converges to the same energies, although somewhat more slowly. These checks give us confidence that our trial function adequately models the nodal surface.

The simulation of bulk systems necessitates the use of periodic boundary conditions to reduce surface effects. The long-range Coulomb interactions between the particles in the simulation cell and their periodic images can then be evaluated by Ewald sums. Periodic boundary conditions require an integer number of wavelengths of the applied field to fit in the simulation cell. The use of multiple oscillations combined with different system sizes allows us to explore the whole range of interesting wave vectors; however, calculation of the long-wavelength behavior ($q \ll k_F$) becomes prohibitively expensive, since the maximum wavelength allowed is proportional to the cube root of the number of particles in the simulation cell.

The QMC dielectric results exhibit significant N dependence and must be extrapolated to the bulk limit. In the study of the ground-state electron gas,[9] the kinetic energy was extrapolated on the basis of the size dependence of noninteracting fermions[20] and the Coulomb potential was corrected for the self-interaction of a particle with its images (a term appropriate to a perfect lattice, but not to a Fermi liquid). Since the calculation of the dielectric by Eq. (2.19) relies solely on energy differences,

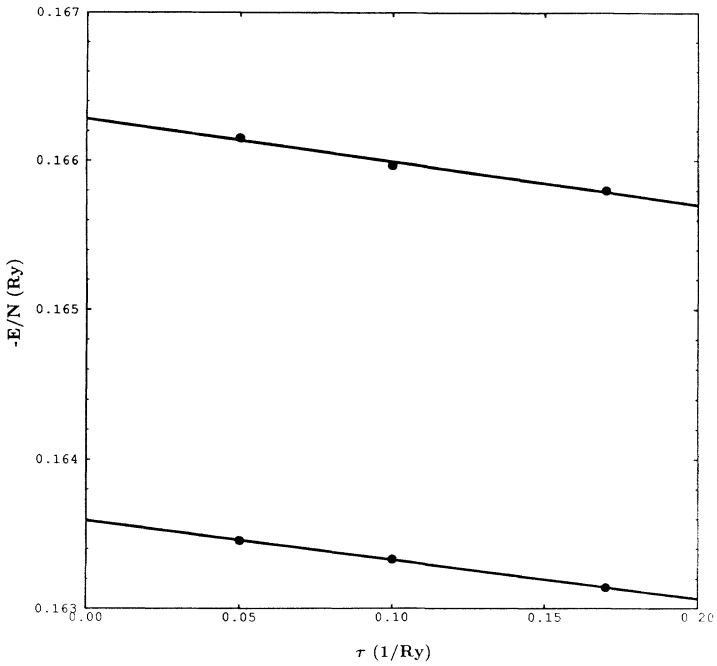

FIG. 1. Time-step τ dependence of the energy for r_s=4, N=54. The straight lines are the best linear fits for the ground state (bottom line) and one applied field, A=0.05 Ry, with wave vector $\mathbf{q}$=[3.09367,0,0] $(1/r_0)$ (lower curve). The error bars are smaller than the symbols.

the Coulomb corrections cancel and the N dependence is determined by the kinetic energy extrapolation. The boson dielectric requires no correction, since the noninteracting Bose gas has no size dependence. For fermions, the extrapolation is based on the number dependence of the $|\mathbf{k}\rangle$ and $|\mathbf{k}^A\rangle$ orbitals. These considerations lead to the following extrapolation scheme, applicable at all wave vectors and densities:

$$\frac{1}{\epsilon_{\mathrm{BULK}}} = \frac{1}{\epsilon_{\mathrm{QMC}}(N)} + \left(\frac{1}{\epsilon_{\mathrm{LIND}}} - \frac{1}{\epsilon_{\mathrm{SCF}}}\right) . \qquad (3.9)$$

We checked the validity of this formula for a given N by comparing the dielectric obtained for two wave vectors of the same norm but different orientation, $(6\pi/L)$ [100] and $(2\pi/L)$ [221], where L is the length of a side of the simulation cell. The discrepancy between the results showed that an additional wave-vector-dependent correction is needed at strongly coupled densities. This was confirmed by simulations using the [111] direction and is in contrast to the conclusion reached in Ref. 12 for the two-dimensional case. The new extrapolation correction is presumably caused by the loss of symmetry due to

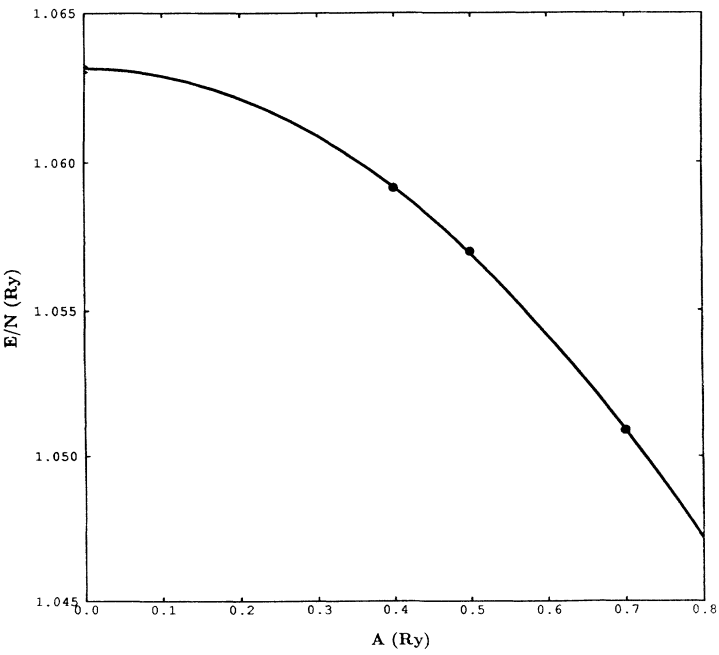

FIG. 2. Diffusion energies vs field strength A, r_s=1, N=54 and wave vector $\mathbf{q}$=[1.03122,0,0] $(1/r_0)$. The curve shows the quadratic fit. The error bars are smaller than the symbols.

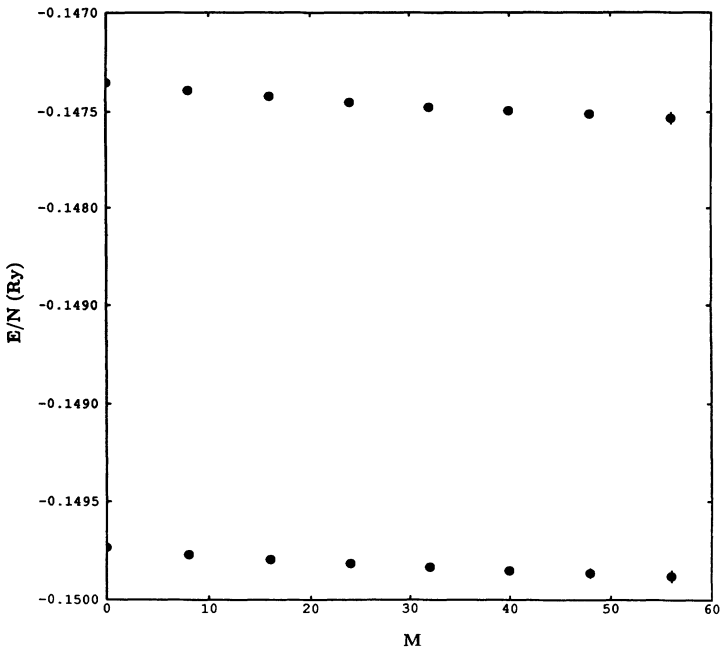

FIG. 3. Released-node energy vs generation after release M for r_s=6, N=38, A=0.0 Ry (top curve), and A=0.035 Ry, with wave vector $\mathbf{q}$=[3.47811,0,0] $(1/r_0)$ (lower curve). The error bars are shown by vertical lines.

the occupation of plane wave orbitals $|\mathbf{k}-\mathbf{q}\rangle$ and $|\mathbf{k}+\mathbf{q}\rangle$, which are not inside the Fermi sphere of the ground state. The loss of symmetry is particularly significant for finite systems, which do not possess the $\mathbf{k}$-space isotropy of the bulk liquid. Because of the shell structure, the wave-vector-dependent correction cannot be obtained by simulating systems of increasing size but constant $\mathbf{q}$. It is smallest for the [100] data, which has the greatest degree of symmetry of the three field orientations considered.

The ground-state bulk extrapolation fit to the finite-N energies is accurate to approximately 0.1%. Since the errors in the energies of the external field systems are no smaller than those for the ground state, the QMC dielectric results have a 10% uncertainty, due to the loss of two significant digits in taking energy differences. Use of a correlated sampling scheme to obtain greater accuracy in the energies would be ineffective, since the finite-N energy differences are already an order of magnitude more precise than the bulk-extrapolated values.

IV. RESULTS

All of the DMC calculations were performed with a time step chosen to yield Metropolis acceptance ratios on the order of 99.3%, which ensures good statistics and convergence. The DMC energies must then be extrapolated to the zero time-step limit. Since the trial wave functions for the ground state and the perturbed systems have different nodal structures, it is not *a priori* obvious that the τ dependencies of the corresponding energies are the same. However, time-dependence plots for the ground-state and applied-field systems show that lines of the same slope can be fit to both, as in the representative plot for $r_s = 4$ shown in Fig. 1. Since the dielectric calculations rely only on energy differences, this means that time-step extrapolation is not required as long as the same τ is used for all field strengths, which results in a considerable computational saving.

A quadratic fit to the constant τ DMC energies is then used to calculate the dielectric function. The greater the number of external fields used, the smaller the resulting statistical error. However, the CPU time required to perform statistically accurate simulations at sufficient choices of densities and wave vectors generally limits us to the use of three to four fields. A typical example of a quadratic fit is illustrated in Fig. 2 for $r_s = 1$, $N = 54$, $\mathbf{q} = [1.031\,22, 0, 0]$, which satisfies

$$E(A)/N = 1.063\,16(6) - 0.0250(2)A^2 \,. \tag{4.1}$$

As a check on the accuracy of DMC, released-node GFMC simulations were performed at $r_s = 6$ for the ground state and one applied field. The GFMC energies as a function of generation after release M are shown in Fig. 3, the energy differences are shown in Fig. 4, and the results are compared with DMC in Table I. The lowering of the ground-state energy from its fixed-node value by $1.8(3) \times 10^{-4}$ Ry (Fig. 3) is consistent with Ceperley and Alder's results[21] of $2(1) \times 10^{-4}$ and $1.0(5) \times 10^{-4}$ Ry at $r_s = 5$ and $r_s = 10$, respectively. (The number in parentheses is the error in the last digit.) Although it does not appear that the released-node calculation has converged in either the ground or perturbed states, the GFMC energy differences as a function of generation after release converge to $-0.002\,35(2)$ Ry for $M > 30$, which is consis-

TABLE I. Comparison of DMC and GFMC energies (in Ry) for $r_s = 6$, N=38, $\mathbf{q}$=[3.47811,0,0] $(1/r_0)$. The error in the last digit is shown in parentheses.

A	$-E_{\mathrm{DMC}}$	$-E_{\mathrm{GFMC}}$	$-\Delta E_{\mathrm{DMC}}$	$-\Delta E_{\mathrm{GFMC}}$
0.0	0.146 98(1)	0.147 48(1)	-	-
0.035	0.149 36(1)	0.149 83(2)	0.002 38(1)	0.002 35(2)

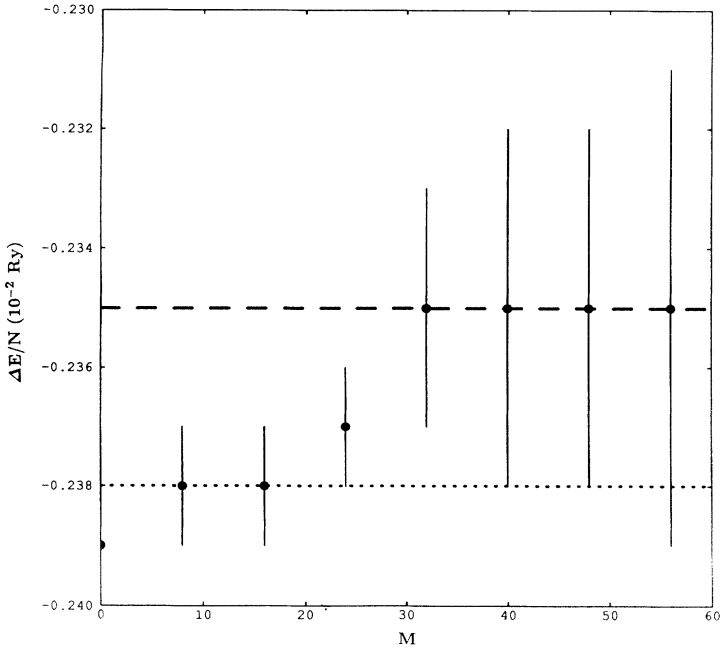

FIG. 4. Released-node energy differences vs generation after release M for r_s=6, N=38 and wave vector q=[3.47811,0,0] $(1/r_0)$. The error bars are shown by vertical lines. The dotted and dashed lines show the diffusion and nodal release energy differences, respectively.

TABLE II. Inverse dielectric response as a function of wave vector q in $(1/r_0)$, $r_s = 1$. $1/\epsilon_N$, $1/\epsilon_D$, $1/\epsilon_{IU}$, $1/\epsilon_{VS}$, and $1/\epsilon_{ASY}$ refer to the finite-N, bulk-extrapolated, Ichimaru-Utsumi, Vashishta-Singwi, and asymptotic compressibility values. All results were obtained with fields in the [100] direction. The error in the last digit is shown in parentheses.

q	N	$1/\epsilon_N$	$1/\epsilon_D$	$1/\epsilon_{IU}$	$1/\epsilon_{VS}$	$1/\epsilon_{ASY}$
0.964 50	66	0.23(1)	0.25(1)	0.243	0.246	0.240
1.031 22	54	0.436(5)	0.286(5)	0.269	0.272	0.269
1.159 37	38	0.300(6)	0.327(6)	0.319	0.324	0.313
1.617 24	14	0.423(2)	0.476(2)	0.485	0.494	-
2.411 59	114	0.717(2)	0.707(2)	0.698	0.712	-
3.093 67	54	0.807(1)	0.815(1)	0.819	0.829	-
4.124 89	54	0.9501(6)	0.9465(6)	0.9459	0.9466	-

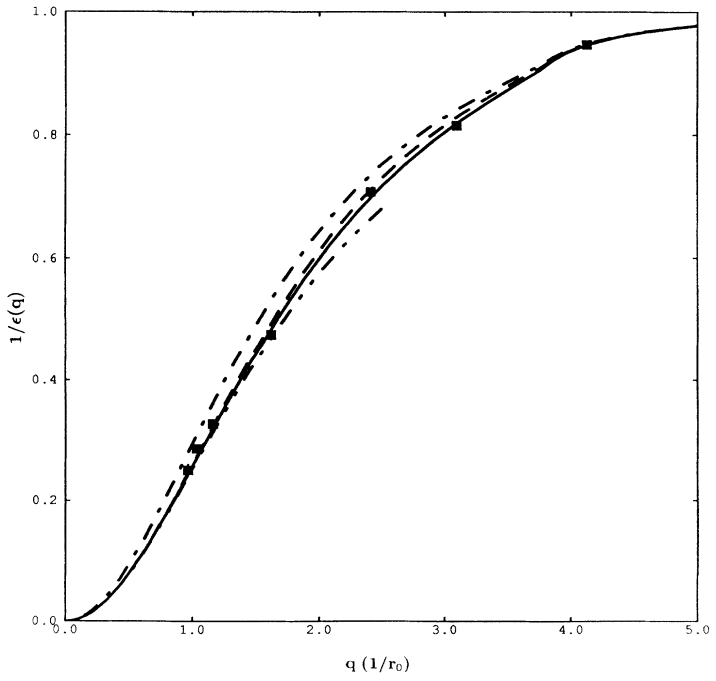

FIG. 5. Inverse dielectric function vs wave vector at $r_s = 1$. The RPA is shown by the dot-dashed line, Vashishta-Singwi by the dashed line, Ichimaru-Utsumi by the solid line, and the low-q asymptote by the double-dotted-dashed line. The diffusion points are shown by squares. The errors are smaller than the symbols.

TABLE III. Inverse dielectric response as a function of wave vector q in $(1/r_0)$, $r_s = 4$. $1/\epsilon_N$, $1/\epsilon_D$, $1/\epsilon_{IU}$, $1/\epsilon_{VS}$, and $1/\epsilon_{ASY}$ refer to the finite-N, bulk-extrapolated, Ichimaru-Utsumi, Vashishta-Singwi, and asymptotic compressibility values. The error in the last digit is shown in parentheses. A * or † indicates a field in the [221] or [111] direction, respectively. All other results were obtained with fields in the [100] direction.

q	N	$1/\epsilon_N$	$1/\epsilon_D$	$1/\epsilon_{IU}$	$1/\epsilon_{VS}$	$1/\epsilon_{ASY}$
0.964 50	66	0.017(2)	0.026(2)	0.024	0.022	0.024
1.031 22	54	0.106(12)	0.031(12)	0.027	0.025	0.027
1.159 37	38	0.024(3)	0.036(3)	0.034	0.034	0.034
1.617 24	14	0.045(6)	0.080(6)	0.067	0.080	0.064
1.786 13	54*	0.09(3)	0.13(3)	0.082	0.104	-
2.008 09	38*	0.26(2)	0.19(2)	0.106	0.143	-
2.145 03	162	0.10(1)	0.12(1)	0.123	0.171	-
	162†	0.19(1)	0.16(1)			-
2.411 59	114	0.246(3)	0.234(3)	0.165	0.233	-
	114†	0.189(6)	0.217(6)			
2.801 14	14*	0.17(1)	0.23(1)	0.246	0.340	-
2.893 50	66	0.328(9)	0.321(9)	0.270	0.367	-
	66†	0.239(6)	0.280(6)			
3.093 67	54	0.338(3)	0.353(3)	0.331	0.429	-
	54†	0.522(5)	0.461(5)			
3.478 11	38	0.560(5)	0.533(5)	0.478	0.555	-
	38†	0.496(6)	0.501(6)			
4.124 89	54	0.7976(7)	0.7868(7)	0.7835	0.7910	-

tent with the DMC value of −0.002 38(1) Ry (see Fig. 4). This indicates that the fixed-node errors cancel upon taking energy differences, although more GFMC simulations would be necessary to establish this point conclusively.

Our QMC results are checked in the asymptotic long-wavelength limit against the compressibility sum rule formula [Eq. (2.7)] using Perdew and Zunger's fit to the ground-state electron gas energies.[22] For the range of r_s studied here, their results are virtually identical to those obtained by Vosko, Wilk, and Nusair.[15] We also compare our values with two dielectric functions from the literature, the Vashishta-Singwi[3] and Ichimaru-Utsumi[6] models described in Sec. II.

At strongly coupled densities, the QMC data are fitted to the Ichimaru-Utsumi form, Eq. (2.11), for $G(q)$, with γ_0 obtained from the fit of Perdew and Zunger mentioned above. The Yasuhara expression Eq. (2.15) for $g(0)$ used in this formula gives values indistinguishable from QMC

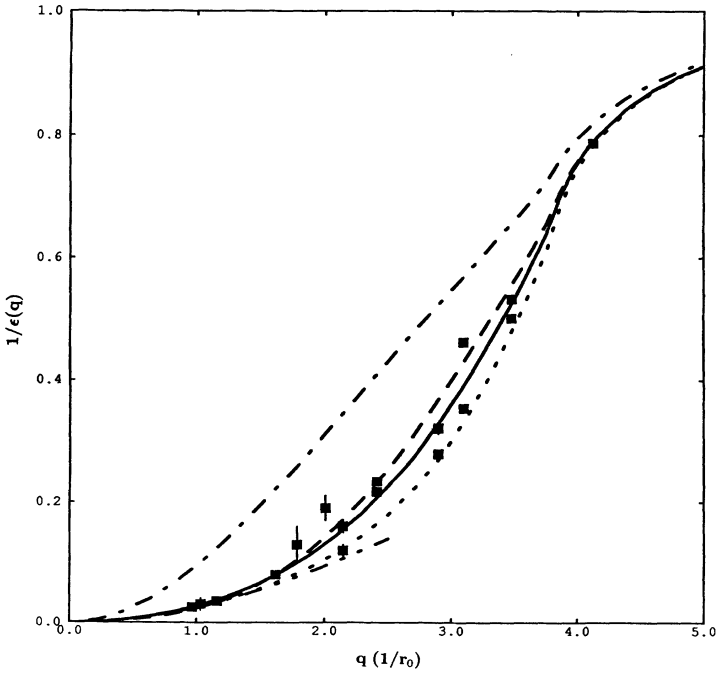

FIG. 6. Inverse dielectric function vs wave vector at $r_s = 4$. The RPA is shown by the dot-dashed line, Vashishta-Singwi by the dashed line, the QMC fit by the solid line, Ichimaru-Utsumi by the dotted line, and the low-q asymptote by the double-dotted-dashed line. The diffusion points are shown by squares and the errors by vertical lines when larger than the symbols.

TABLE IV. Inverse dielectric response as a function of wave vector q in $(1/r_0)$, $r_s = 6$. $1/\epsilon_N$, $1/\epsilon_D$, $1/\epsilon_{IU}$, $1/\epsilon_{VS}$, and $1/\epsilon_{ASY}$ refer to the finite-N, bulk-extrapolated, Ichimaru-Utsumi, Vashishta-Singwi, and asymptotic compressibility values. The error in the last digit is shown in parentheses. A $*$ or † indicates a field in the [221] or [111] direction, respectively. All other results were obtained with fields in the [100] direction.

q	N	$1/\epsilon_N$	$1/\epsilon_D$	$1/\epsilon_{IU}$	$1/\epsilon_{VS}$	$1/\epsilon_{ASY}$
1.031 22	54	0.06(1)	0.00(1)	-0.012	-0.016	-0.012
1.617 24	14	-0.048(7)	-0.021(7)	-0.032	-0.020	-0.029
1.786 13	54*	-0.06(1)	-0.03(1)	-0.038	-0.016	-
2.008 09	38*	0.127(7)	0.062(7)	-0.047	-0.004	-
2.145 03	162	-0.030(5)	-0.013(5)	-0.051	0.007	-
	162†	0.033(5)	0.014(5)			
2.411 59	114	0.063(4)	0.053(4)	-0.053	0.041	-
	114†	-0.010(7)	0.015(7)			-
2.801 14	14*	-0.070(7)	-0.005(7)	-0.029	-0.123	-
2.893 50	66	0.109(4)	0.103(4)	-0.015	0.148	-
	66†	-0.006(7)	0.033(7)			-
3.093 67	54	0.087(3)	0.101(3)	0.032	0.209	-
	54†	0.317(4)	0.254(4)			-
3.478 11	38	0.358(3)	0.330(3)	0.202	0.356	-
	38†	0.292(5)	0.297(5)			-
4.124 89	54	0.687(1)	0.673(1)	0.674	0.685	-

results within statistics. The free parameter a is determined by least-squares optimization to the [100] QMC data, which exhibits the smallest size dependence of the three field orientations. Values of the fit parameters a, γ_0, and $g(0)$ are given in Table VI. Using QMC data for $S(k)$ in the hypernetted-chain self-consistency relation Eq. (2.16) gives a $G(k)$ curve which does not fit the QMC data as well as the Ichimaru-Utsumi parametrized form.

A. Weakly coupled fluid — $r_s = 1$

Table II gives results for the finite-N and bulk-extrapolated DMC [(Eq. (3.9)] dielectric function, together with numbers derived from the Ichimaru-Utsumi and Vashishta-Singwi local-field corrections, and the asymptotic values obtained from the GFMC compressibility. The same data is plotted in Fig. 5, together with the RPA dielectric function. It should be noted that the

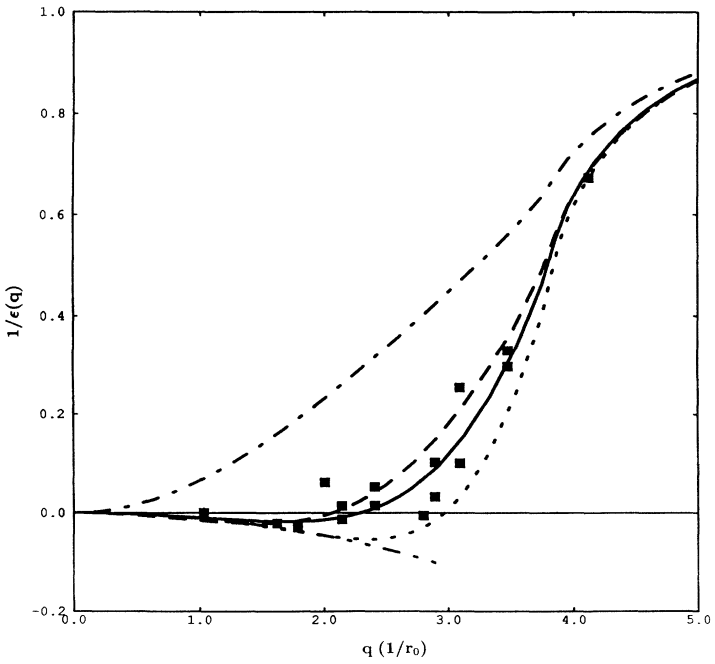

FIG. 7. Inverse dielectric function vs wave vector at $r_s = 6$. The RPA is shown by the dot-dashed line, Vashishta-Singwi by the dashed line, the QMC fit by the solid line, Ichimaru-Utsumi by the dotted line and the low-q asymptote by the double-dotted-dashed line. The diffusion points are shown by squares. The errors are smaller than the symbols.

TABLE V. Inverse dielectric response as a function of wave vector q in $(1/r_0)$, $r_s = 10$. $1/\epsilon_N$, $1/\epsilon_D$, $1/\epsilon_{IU}$, and $1/\epsilon_{ASY}$ refer to the finite-N, bulk-extrapolated, Ichimaru-Utsumi, and asymptotic values. The error in the last digit is shown in parentheses. A * or † indicates a field in the [221] or [111] direction, respectively. All other results were obtained with fields in the [100] direction.

q	N	$1/\epsilon_N$	$1/\epsilon_D$	$1/\epsilon_{IU}$	$1/\epsilon_{ASY}$
1.031 22	54	0.003(2)	-0.033(2)	-0.049	-0.047
1.238 43	162*	-0.038(7)	-0.052(7)	-0.072	-0.070
1.617 24	14	-0.118(3)	-0.100(3)	-0.132	-0.125
1.786 13	54*	-0.145(4)	-0.123(4)	-0.167	-
2.008 09	38*	-0.049(4)	-0.098(4)	-0.222	-
2.411 52	114	-0.177(8)	-0.186(8)	-0.346	-
2.801 14	14*	-0.351(7)	-0.297(7)	-0.477	-
2.893 50	66	-0.233(6)	-0.238(6)	-0.502	-
	66†	-0.347(6)	-0.313(6)		-
3.093 67	54	-0.228(2)	-0.215(2)	-0.534	-
	54†	-0.012(3)	-0.071(3)		-
3.478 11	38	0.065(3)	0.036(3)	-0.405	-
4.124 89	54	0.487(1)	0.470(1)	0.450	-

QMC number-dependence correction from Eq. (3.9) is substantial ($\approx 52\%$ for $q = 1.03122$). The QMC results are consistent with the low-q asymptote, even at wavelengths for which the compressibility sum rule is not expected to be accurate. The RPA underestimates the correct response at all wave vectors, although the coupling is relatively weak. The bulk-extrapolated QMC results closely correspond with the two other dielectric models over the entire range of wave vectors.

B. Metallic fluid — $r_s = 4$

Accurate calculations in the density regime typical of alkali metals—Na ($r_s = 3.93$), K ($r_s = 4.86$), Cs ($r_s = 5.62$)—are of considerable interest. The QMC data for $r_s = 4$ are given in Table III. The two sets of QMC points at intermediate wave vectors correspond to the [100] and [221] orientations, the latter indicated by a * in the table. Additional wave vectors, with the field oriented along the [111] diagonal, are indicated by a †. The same data are plotted in Fig. 6, together with the RPA, the Vashishta-Singwi and Ichimaru-Utsumi curves, the long-wavelength asymptote, and the QMC fit (Table VI). As the figure shows, the number correction works well at long wavelengths, where the local-field correction is small, but cannot eliminate all the size effects at intermediate wave vectors. As expected, the RPA is now a poor description of the induced charge, severely underestimating the dielectric response over the entire range

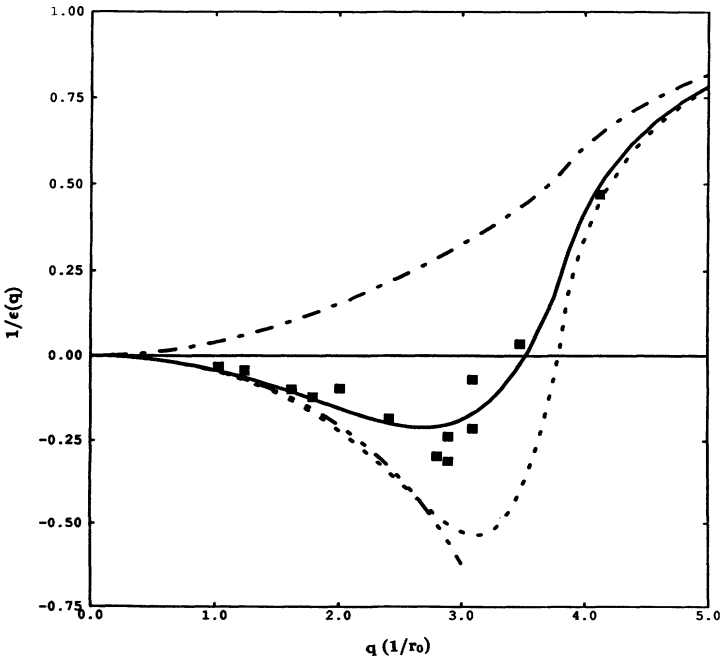

FIG. 8. Inverse dielectric function vs wave vector at $r_s = 10$. The RPA is shown by the dot-dashed line, the QMC fit by the solid line, Ichimaru-Utsumi by the dotted line and the low-q asymptote by the double-dotted-dashed line. The diffusion points are shown by squares. The errors are smaller than the symbols.

of wave vectors. The QMC fit is approximately bounded by the two other curves, indicating that the response at this density lies in between the corresponding theories.

C. Low-density metallic fluid — $r_s = 6$

The electron gas compressibility becomes negative for $r_s \gtrsim 5.24$. As a consequence, the low-density metallic fluid exhibits striking differences from the behavior at higher densities. The QMC data and the various dielectric model values are given in Table IV and plotted in Fig. 7, together with the QMC fit (Table VI). The dielectric response becomes arbitrarily large and negative at low q, which is consistent with the compressibility sum rule, Eq. (2.7). Another distinctive feature is the appearance of an infinite discontinuity in the dielectric where the sign of $1/\epsilon$ changes near $q = 2.0 \approx k_F$. The RPA is completely inadequate at this density, predicting a positive response over the entire range of wave vectors. Comparison with the QMC fit shows that the Vashishta-Singwi curve appears qualitatively correct in the region of the axis-crossing discontinuity. By contrast, the Ichimaru-Utsumi theory substantially misses the location of the sign change and lies below the QMC data at intermediate wave vectors. As before, the two models act as approximate bounds to the QMC fit.

D. Strongly interacting fluid — $r_s = 10$

The results at $r_s = 10.0$ are qualitatively similar to those at $r_s = 6.0$, due to the negative compressibility of the fluid. The QMC data are given in Table V and plotted in Fig. 8, together with the RPA, the Ichimaru-Utsumi function, the QMC fit (Table VI), and the long-wavelength asymptote. No data are available for the Vashishta-Singwi dielectric at this density. The magnitude of the response and the wave vector at the change of sign differ significantly from the Ichimaru-Utsumi values.

TABLE VI. Local-field correction fitting parameters.

r_s	a	γ_0	$g(0)$
4	0.011	0.2810	0.0533
6	0.012	0.2915	0.0213
10	0.003	0.3074	0.0042

V. SUMMARY

Our QMC results represent a first-principles calculation of the static dielectric function of the three-dimensional electron gas and provide a useful benchmark for future work. The data agree with the asymptotic limits, and are bounded by established dielectric theories at intermediate wave vectors. In principle, the same method can be used to calculate the macroscopic dielectric function of any solid-state system, metallic or insulating. The essential difficulty of the approach lies with the bulk-extrapolation problem which requires either simulations of significantly larger systems or the development of an improved extrapolation formula.

ACKNOWLEDGMENTS

The authors would like to thank K. Runge for reading the paper and providing useful comments, and D. Ceperley for correspondence on the ground-state extrapolation. This work was performed under the auspices of the U.S. Department of Energy Lawrence Livermore National Laboratory Contract No. W-7405-ENG-48.

*Present address: Centre d'Étude de Limeil, Villeneuve-St-George, France.

[1] D.J.W. Geldart and R. Taylor, Can. J. Phys. **44**, 2137 (1966); F. Toigo and T.O. Woodruff, Phys. Rev. B **2**, 3958 (1970).
[2] F. Brosens, J.T. Devreese, and L.F. Lemmens, Phys. Rev. B **21**, 1363 (1980); K. Utsumi and S. Ichimaru, *ibid.* **22**, 1522 (1980).
[3] P. Vashishta and K.S. Singwi, Phys. Rev. B **6**, 875 (1972).
[4] K. Utsumi and S. Ichimaru, Phys. Rev. B **22**, 5203 (1980); **24**, 3220 (1981).
[5] V.D. Gorobchenko and E.G. Maksimov, Usp. Fiz. Nauk. **130**, 65 (1980) [Sov. Phys. Usp. **23**, 35 (1980)].
[6] S. Ichimaru and K. Utsumi, Phys. Rev. B **24**, 7385 (1981).
[7] L. Lantto, P. Pietiläinen, and A. Kallio, Phys. Rev. B **26**, 5568 (1982).
[8] P. Pietiläinen and A. Kallio, Phys. Rev. B **27**, 224 (1983).
[9] D.M. Ceperley and B.J. Alder, Phys. Rev. Lett. **45**, 566 (1980).
[10] D.M. Ceperley and B.J. Alder, Phys. Rev. B **36**, 2092 (1987); G. Sugiyama, G. Zerah, and B.J. Alder, Physica A **156**, 144 (1989).
[11] G. Sugiyama, C. Bowen, and B.J. Alder, Phys. Rev. B **46**, 13 042 (1992).
[12] S. Moroni, D. Ceperley, and G. Senatore, Phys. Rev. Lett. **69**, 1837 (1992).
[13] J.C. Kimball, Phys. Rev. A **7**, 1648 (1973).
[14] D. Pines and P. Nozières, *The Theory of Quantum Liquids* (Benjamin, New York, 1966), Vol 1.
[15] S.H. Vosko, L. Wilk, and M. Nusair, Can. J. Phys. **58**, 1200 (1980).
[16] H. Yasuhara, Solid State Commun. **11**, 1481 (1972).
[17] D.M. Ceperley, Phys. Rev. B **18**, 3126 (1978).
[18] P. Reynolds, D. Ceperley, B.J. Alder, and W. Lester, J. Chem. Phys. **77**, 5593 (1982).
[19] D.M. Ceperley and B.J. Alder, J. Chem. Phys. **81**, 5833 (1984).
[20] D. Ceperley, G.V. Chester, and M.H. Kalos, Phys. Rev. B **16**, 3081 (1977).
[21] From *Recent Progress in Many-Body Theories*, edited by J.G. Zabolitzky *et al.* (Springer-Verlag, New York, 1981).
[22] J.P. Perdew and A. Zunger, Phys. Rev. B **23**, 5048 (1981).